Nonmonotonic heat dissipation phenomenon in close-packed hotspot systems

Chuang Zhang [*] and Lei Wu [†]

Department of Mechanics and Aerospace Engineering, Southern University of Science and Technology, Shenzhen 518055, China

(Received 16 March 2022; revised 7 June 2022; accepted 21 June 2022; published 11 July 2022)

Transient heat dissipation in close-packed quasi-two-dimensional nanoline and three-dimensional nanocuboid hotspot systems is studied based on the phonon Boltzmann transport equation. It is found that, counterintuitively, the heat dissipation efficiency is not a monotonic function of the distance between adjacent nanoscale heat sources but reaches the highest value when this distance is comparable to the phonon mean free path. This is due to the competition of two thermal transport processes: quasiballistic transport when phonons escape from the nanoscale heat source and the scattering among phonons originating from the adjacent nanoscale heat source.

DOI: 10.1103/PhysRevE.106.014111

I. INTRODUCTION

With the fast development of micro- and nanotechnologies [1–3] and the drastically reduced size of electronic devices [3,4], Moore's law is reaching its limit. In addition, the increase of power density intensifies hotspot issues and increases the demand for heat dissipation. The heat dissipation problem at the micro- and nanoscales has become one of the key bottlenecks restricting the further development of the microelectronics industry. Hence, it is important to understand the thermal transport mechanisms in microelectronic devices [3,5,6] to realize optimal waste heat removal and improve device performance and reliability.

At the micro- and nanoscales, the Fourier law of thermal conduction becomes invalid and the non-Fourier phonon transport is summarized into four major categories [1,2,4,7,8]. The first is the ballistic phonon transport [9–11], which happens when the system's characteristic length or time is much shorter than the phonon mean free path [12–15] or relaxation time [16–18]. The second arises from small-scale heat sources [19–25]. When a hotspot with small size is added in a bulk material, if the phonon mean free path is much larger than the size of the hotspot, phonons emitted from the hotspot do not suffer sufficient phonon-phonon scattering near the hotspot region so quasiballistic phonon transport occurs even if there is no boundary or interface scattering inside the systems [21,22,24]. The third is the coherent phonon transport [26–28], which appears when the system's characteristic length is comparable to the phonon wavelength. The fourth is the hydrodynamic phonon transport, which requires the momentum-conserved normal scattering to be much more extensive than the boundary scattering and the boundary scattering to be much more sufficient than the momentum-destroying resistive scattering [29–31]. So far, the phonon hydrodynamics phenomena have been experimentally measured in a few three-dimensional (3D) materials (e.g., graphite and NaF) at low temperatures [31–33].

Except for the above situations, recent studies have revealed the importance of the distance between adjacent nanoscale heat sources on the heat dissipation in hotspot systems [34–38]. Zeng and Chen [36] studied quasiballistic heat conduction for quasi-2D nanoline heat sources, which are periodically deposited on a substrate. Based on the frequency-independent phonon Boltzmann transport equation (BTE) under the relaxation time approximation, they found that the collective behavior caused by closely packed hotspots could counteract the quasiballistic effects in an isolated nanoscale hotspot. However, the result depends on which temperature signal is used as the fitting data of the diffusion equation. Hoogeboom-Pot *et al.* measured this unexpected phenomenon by advanced dynamic extreme ultraviolet scatterometry [34]. To reveal a comprehensive microscopic understanding of this unexpected heat dissipations, Honarvar *et al.* [38] performed the steady-state molecular dynamics simulations on silicon samples featuring close-packed nanoheaters. They made a qualitative comparison between the molecular dynamics simulations and extreme ultraviolet experiments by controlling the equal ratio between the phonon mean free path and geometry size. By using atomic-level simulations to accurately access the temperature, phonon scattering, and transport properties, they explained that the phonons emitted from the nanoscale heat source may scatter with each other in the in-plane direction and promote the cross-plane heat dissipation when the distance between two nanoscale heat sources is smaller than the phonon mean free path. This heat dissipation phenomenon was also reported by Minnich and co-workers resulting from the phonon BTE and time-domain thermoreflectance experiments [39,40]. Those results suggest that heat dissipation or cooling in nanoscale hotspot systems including integrated circuits [3,5] might not be as challenging as previously expected.

However, the fundamental physical mechanisms of this phenomenon are still not unified. In addition, it is worth noting

[*] zhangc33@sustech.edu.cn
[†] Corresponding author: wul@sustech.edu.cn

that various macroscopic constitutive relationships between the heat flux and temperature have been used to fit the experimental data by different research groups [34,36,37,40]. By artificial fitting, an effective thermal conductivity can be obtained, which varies nonmonotonically when the distance between the nanoscale hotspot decreases gradually. Usually, the heat diffusion equation with a constant effective thermal conductivity is widely used during data postprocessing, as done by Hoogeboom-Pot *et al.* [34] and Zeng and Chen [36], but this model cannot simultaneously fit both the amplitude and phase well [37,39,40]. Under the semi-infinite assumption, Hua and Minnich [40] obtained a constitutive relationship between the heat flux and temperature by analytically deriving the phonon BTE under the relaxation time approximation, which is valid for all phonon transport regimes. However, this analytical strategy is very challenging for complex geometries and hotspot systems with finite size. Beardo *et al.* used a macroscopic moment equation with adjustable parameters to fit the experimental data, and both the nonlinear and nonlocal terms of the heat flux are taken into account in their model [37]. They uncovered the existence of two timescales: an interface resistance regime that dominates on short timescales and a quasiballistic phonon transport regime that dominates on longer timescales. This moment equation is derived from the phonon BTE under the small-perturbation expansion, so it might be questionable when the system size is smaller than the phonon mean free path.

Summing up the above, it seems that how to interpret the raw experimental data in the nondiffusive regime with reasonable constitutive relationships is still an open question. As reported by Zeng and Chen [36], using the temperature signals in different positions for data postprocessing might lead to different result. Hence, it is necessary to obtain the macroscopic physical fields in the whole domain.

Note that there are only a few detection sites in the micro- and nanoscale thermal measurement experiments [11,16,21,22,24,34,38,39], which indicates that it is hard to measure the whole temporal and spatial macroscopic physical fields. On the other hand, as is well known, heat dissipation in practical thermal engineering spans multiple scales of time and space, for example, from picoseconds to microseconds or from transistors at the nanoscale to the heat dissipation of a supercomputer [5]. Although the molecular dynamics simulation is accurate, it is still too expensive to simulate the dimensions and scales of actual experimental samples or thermal systems. For example, in the work of Honarvar *et al.* [38], the transient extreme ultraviolet experiment is usually at hundreds of nanometers, but the steady-state molecular dynamics simulation is below 100 nm.

The phonon incoherent transport dominates heat conduction in room temperature silicon over tens of nanometers [28,36,39–42]. Simultaneously considering the accuracy and computational efficiency, the phonon BTE simulations are conducted in our work to show the temporal and spatial variations of macroscopic physical fields in the whole 3D finite geometry region. We mainly focus on how long it takes for the heat to dissipate completely from the heat source. No artificial fitting or effective thermal conductivity is used to avoid possible controversy caused by data postprocessing methods and the raw data calculated by the phonon BTE are plotted directly.

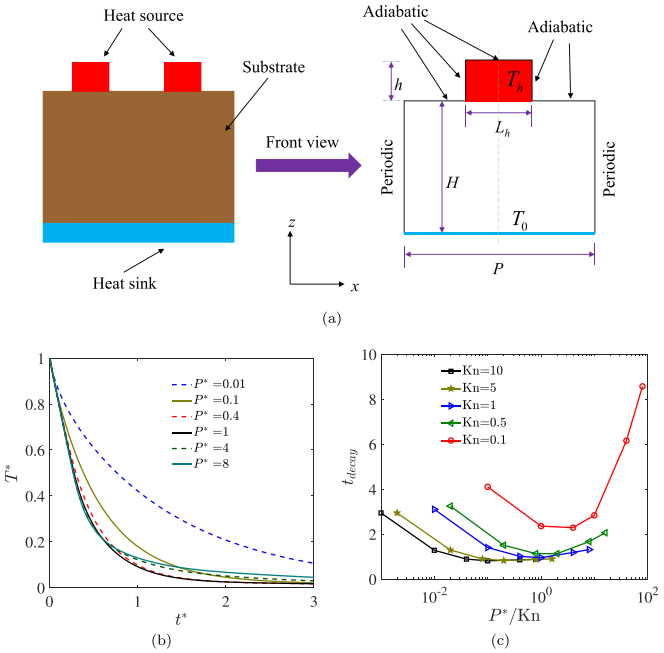

FIG. 1. (a) Schematic of the transient heat dissipation in a quasi-2D nanoline heat source with a periodic array arrangement. (b) Heat dissipation process of the average temperature (7) based on the gray model, where Kn = 1.0. (c) Time decay t_{decay} with various P^* and Kn.

The rest of the paper is organized as follows. In Sec. II the phonon BTE is introduced. The results and discussion of quasi-2D nanoline [Fig. 1(a)] and 3D nanocuboid [Fig. 4(a)] hotspot systems are given in Sec. III and IV, respectively. A summary is given in Sec. V.

II. PHONON BTE

In this work we mainly focus on the heat conduction in conventional 3D semiconductor materials, e.g., monocrystalline silicon and germanium [39,40,43,44]. In these materials, the normal process scattering can be ignored and the resistive process scattering dominates the heat conduction [18,36,39,40,43]. The phonon BTE under the relaxation time approximation [10,17,18,40,41,45,46] is used to describe the transient heat conduction in these materials

$$\frac{\partial e}{\partial t} + v_g \boldsymbol{s} \cdot \nabla_{\boldsymbol{x}} e = \frac{e^{\text{eq}} - e}{\tau}, \tag{1}$$

where v_g is the group velocity and $e = e(\boldsymbol{x}, \omega, \boldsymbol{s}, t, p)$ is the phonon distribution function of energy density, which depends on spatial position $\boldsymbol{x}$, unit directional vector $\boldsymbol{s}$, time t, phonon frequency ω, and branch p (Appendix A). The whole wave-vector space is assumed to be isotropic. In addition, e^{eq} and τ are the equilibrium distribution function and the relaxation time, respectively. We assume that the temperature T slightly deviates from the reference temperature T_0, i.e., $|T - T_0| \ll T_0$, so that the equilibrium distribution function

can be linearized as

$$e_R^{\rm eq}(T) \approx C\frac{T - T_0}{4\pi}, \tag{2}$$

where $C = C(\omega, p, T_0)$ is the mode specific heat at T_0. The phonon scattering term satisfies the energy conservation, so we have

$$0 = \sum_p \iint \frac{e^{\rm eq}(T_{\rm loc}) - e}{\tau(T_0)} d\Omega\, d\omega, \tag{3}$$

where the integral is carried out in the whole solid angle space $d\Omega$ and frequency space $d\omega$. Here $T_{\rm loc}$ is the local pseudotemperature, which is introduced to ensure the conservation principles of the scattering term and can be calculated by

$$T_{\rm loc} = T_0 + \frac{\sum_p \int \frac{\int e\, d\Omega}{\tau} d\omega}{\sum_p \int \frac{C}{\tau} d\omega}. \tag{4}$$

The local temperature T and heat flux $\boldsymbol{q}$ can be calculated as the moments of the distribution function

$$T = T_0 + \frac{\sum_p \int\int e\, d\Omega\, d\omega}{\sum_p \int C\, d\omega}, \tag{5}$$

$$\boldsymbol{q} = \sum_p \iint \boldsymbol{v} e\, d\Omega\, d\omega. \tag{6}$$

III. QUASI-2D NANOLINE HEAT SOURCE

A. Problem description

The heat dissipations in quasi-2D nanoline hotspot systems are investigated numerically. As shown in Fig. 1(a), a heat source is added on the top of a rectangle substrate and its sizes in the x and z directions are L_h and h, respectively. The sizes of the substrate in the x and z directions are P and H, respectively. The bottom of the substrate is the heat sink with environment temperature T_0 and the isothermal boundary condition is used [Eq. (B2)]. The left and right boundaries of the substrate are periodic and the others are diffusely reflecting adiabatic boundaries [Eq. (B3)]. We set $h/H = 1/8$ and $L_h/P = 1/4$, and the whole domain is a homogeneous material in order to eliminate the thermal interface resistance between two dissimilar materials [47,48].

At the initial moment $t = 0$, the temperature of the heat source and the other areas are T_h and T_0, respectively, where $T_h > T_0$. When $t > 0$, the heat dissipates from the heat source to the heat sink. The temporal evolutions of the average temperature $\overline{T}$ are studied based on the phonon BTE

$$T^* = \frac{\overline{T} - T_0}{T_h - T_0}, \tag{7}$$

where $\overline{T}$ is the average temperature over the whole heat source. We mainly focus on how long it takes for heat to dissipate completely from the heat source. Specifically, we study the factors that influence the time decay $t_{\rm decay}$, which is defined as the time cost when T^* decreases from 1.0 to 0.1. Based on dimensional analysis [49], the transient heat dissipations in the quasi-2D nanoline hotspot systems are totally determined by these length scales, including the phonon mean free path $\lambda = v_g\tau$, the spatial period P, the height H, and the size of the hotspot L_h. Equation (1) can be written in the dimensionless form

$$\frac{\partial e}{\partial t} + \boldsymbol{s}\cdot\nabla_{\boldsymbol{x}} e = \frac{e^{\rm eq} - e}{\rm Kn}, \tag{8}$$

where the distribution function is normalized by $e_{\rm ref} = C\Delta T/4\pi$, with $\Delta T = T_h - T_0$ the temperature difference in the domain, the spatial coordinates normalized by H, and time normalized by $t_{\rm ref} = H/v_g$. The dimensionless Knudsen number is

$${\rm Kn}^{-1} = \frac{H}{\lambda} = \frac{H}{v_g\tau}. \tag{9}$$

In order to better pinpoint the relationships among various influencing factors, two dimensionless parameters are introduced and are defined as

$$P^* = \frac{P}{H}, \quad t^* = \frac{v_g t}{H}. \tag{10}$$

B. Effects of geometric sizes and phonon scattering

The phonon gray model [36,41] and the linear phonon dispersion are used. In this simulation, the height H is fixed. Detailed numerical solutions of the BTE are shown in Appendix B and the independence test is conducted in Appendix C.

The thermal effects of the spatial period P are investigated. As shown in Fig. 1(b) with ${\rm Kn} = 1.0$, the heat dissipation efficiency is not monotonic when P^* decreases from 8 to 0.01. The time decay $t_{\rm decay}$ is also plotted in Fig. 1(c). When $P^* =$ 1.0 or 0.4, the heat dissipation speed is the fastest. Note that both v_g and H are fixed when the spatial period P changes, so the dimensionless time t^* is equivalent to the actual physical time t.

Next a number of simulations are carried out with various Kn. It can be found that the nonmonotonic heat dissipation phenomenon still exists with different Knudsen numbers. The present results clearly contradict the previous intuitive understanding of micro- and nanoscale heat transfer, namely, the more densely packed and smaller the electronics, the more difficult it is to dissipate heat [3,5].

C. Physical mechanisms

Motivated by previous studies of quasiballistic phonon transport [20,34,36,38–40], the fundamental physical mechanisms of the above unexpected thermal transport phenomena in different phonon transport regimes are discussed qualitatively. From Fig. 1(a) or 2 it can be found that there are two main thermal transport processes when heat is transferred from the heat source to the heat sink [34,36]: Phonons escape from the heat source to the substrate and phonons are transported from the substrate to the heat sink. Based on dimensionless analysis [49], for the first process, the size of the heat source is the key factor, especially L_h/h. For the second process, namely, when phonons with high energy are absorbed by the heat sink, the distance P between the nanoscale heat source and height H determines the heat dissipation efficiency. In addition, the phonon group velocity and relaxation time influence both transient heat dissipation processes.

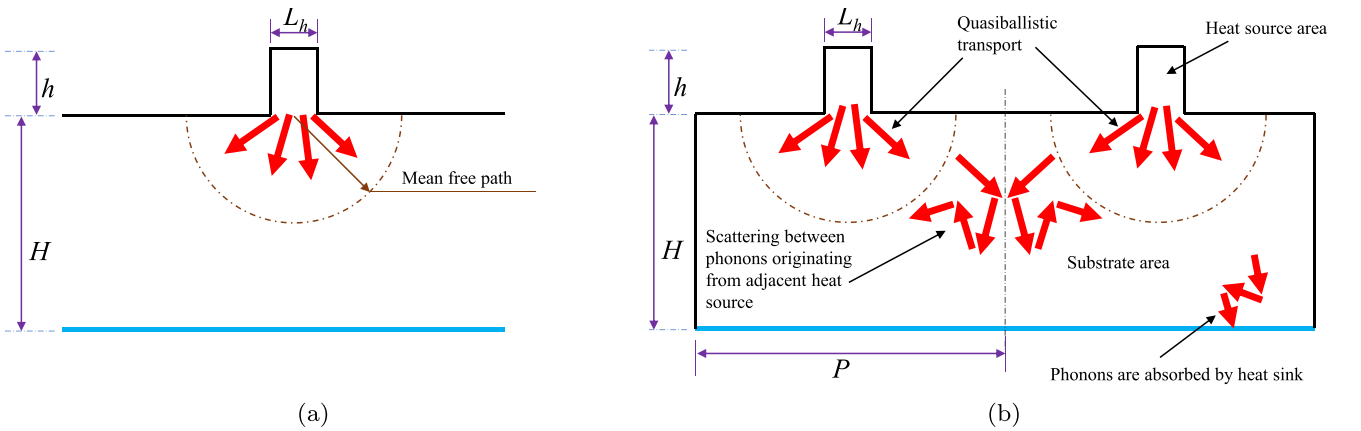

FIG. 2. Schematic of phonon transport and scattering in (a) a single hotspot and (b) close-packed hotspot systems.

1. Diffusion

When the spatial period is much larger than the phonon mean free path, $P \gg \lambda$ and $L_h \gg \lambda$, the phonon scattering is sufficient inside both the heat source and substrate areas and phonons undergo a diffusive process. Hence, Fourier's law is valid and the temperature decreases exponentially.

2. Quasiballistic transport

When the spatial period decreases and becomes comparable to the phonon mean free path, the thermal dissipation mechanisms become much complicated. For the first process, L_h/h decreases so that it becomes difficult for phonons to escape from the heat source areas. For the second process, if there is only a single nanoscale heat source, as shown in Fig. 2(a), when phonons escape from the heat source, there is rare phonon-phonon scattering within the spatial range of a phonon mean free path. The insufficient phonon scattering blocks the efficient energy exchange among phonons and a large thermal resistance appears near the outlet position of the heat source [8,20].

When a number of heat sources are periodically deposited on a substrate, it should be noted that the distance between two nanoscale heat sources decreases if P decreases. The phonons that escape from one nanoscale heat source may scatter with others that escape from the adjacent heat source. In other words, when the distance between two nanoscale heat sources decreases and $P \approx \lambda$, compared to that with a single nanoscale hotspot, the probability of actual phonon scattering is instead boosted within the spatial range of a phonon mean free path, as shown in Fig. 2(b). The heat flux in the x direction is canceled out by phonons coming from opposite directions. In addition, the heat conduction in the z direction is increased, which is totally different from that of a single nanoscale heat source [34,38].

3. Ballistic transport

When the spatial period is much smaller than the phonon mean free path, $P \ll \lambda$ and $L_h \ll \lambda$, the ballistic phonon transport dominates heat conduction inside both the heat source and substrate areas. Although the smaller distance between two nanoscale heat sources could promote scattering, the ratio L_h/h decreases significantly so that the phonon transport is blocked by the diffusely reflecting boundaries and it is very difficult for most of the heat and phonons to escape from the heat source to the substrate areas. In other words, the first process totally dominates phonon transport and limits the heat dissipation.

Combined with our numerical results in Fig. 1 and the theoretical analysis of quasiballistic phonon transport [34,36,38],

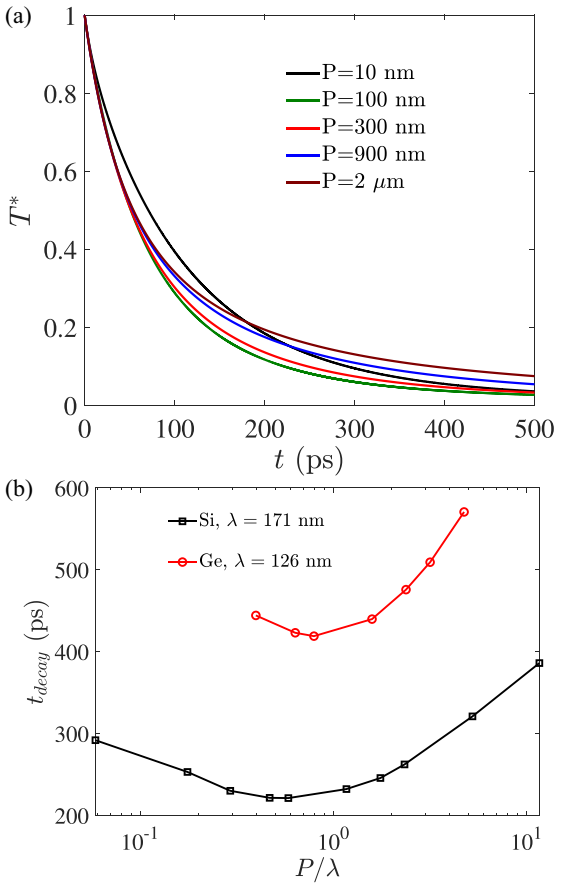

FIG. 3. (a) Heat dissipation process of the average temperature (7) in silicon materials with quasi-2D nanoline geometry [Fig. 1(a)] based on the frequency-dependent BTE, where $H = 300$ nm and $T_0 = 300$ K. (b) Time decay t_{decay} with various P in silicon and germanium materials.

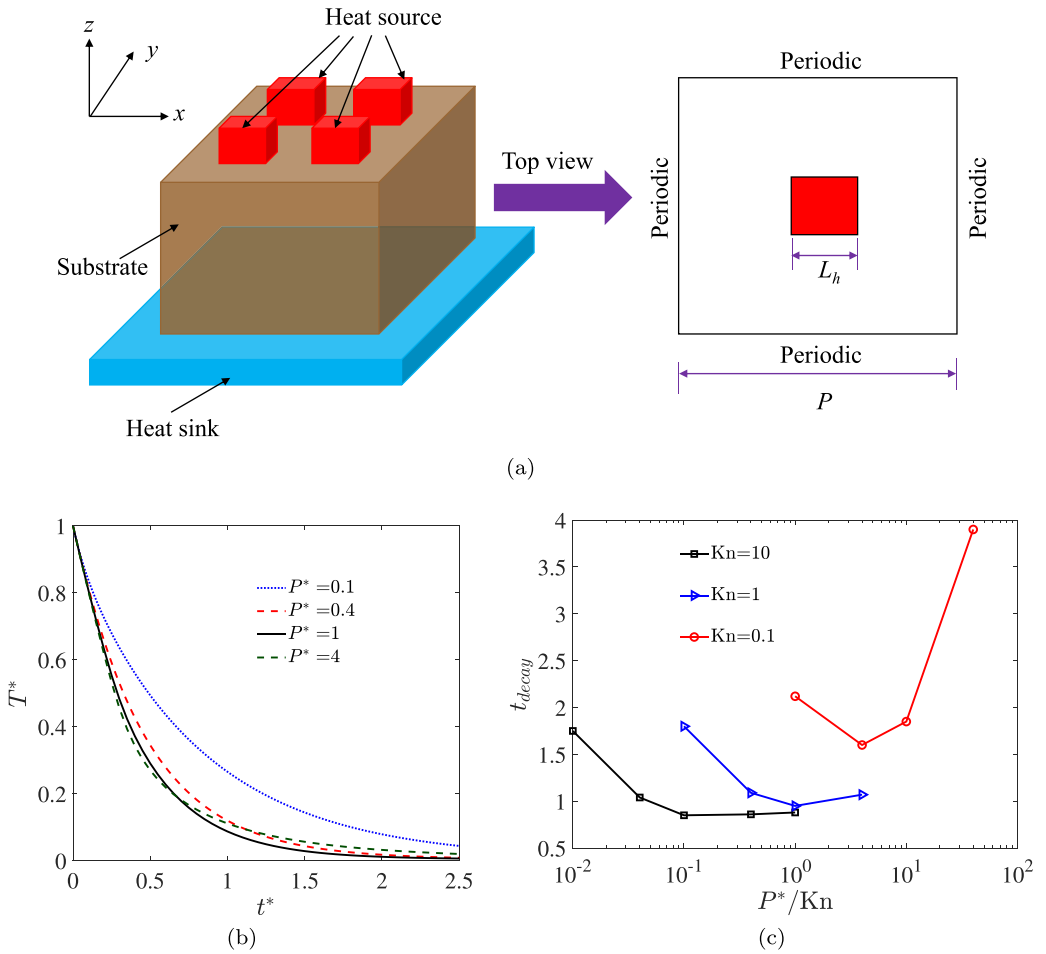

FIG. 4. (a) Schematic of the transient heat dissipation in a 3D nanocuboid heat source with a periodic array arrangement. (b) Heat dissipation process of the average temperature (7) based on the gray model, where Kn = 1. (c) Time decay t_{decay} with various P^* and Kn.

it is concluded that in quasi-2D hotspot systems, the heat dissipation efficiency reaches the highest value when $P^*/\text{Kn} \approx 1$. It is a result of the competition between the two phonon transport processes: quasiballistic transport when phonons escape from the nanoscale heat source and the scattering among phonons originating from the adjacent nanoscale heat source.

D. Silicon and germanium materials

The quasi-2D nanoline hotspot systems [Fig. 1(a)] with room temperature monocrystalline silicon and germanium materials are studied based on frequency-dependent phonon BTE. The input parameters of the BTE including nonlinear phonon dispersion and frequency-dependent scattering processes are given in Appendix A, which have been validated by experiments in previous studies [43,44,50]. The average phonon mean free path $\lambda = \sum_p \int C v_g^2 \tau \, d\omega / \sum_p \int C v_g d\omega$ of room temperature silicon is about 171 nm. The thermal effects of the spatial period P on the heat dissipation are investigated and the height is fixed at $H = 300$ nm [38]. From Figs. 3(a) and 3(b) it can be found that in silicon the heat dissipation efficiency is low when $P = 2\ \mu$m or 10 nm and the efficiency is the fastest when $P \approx 100$ nm. Similar nonmonotonic heat dissipation phenomena are also observed in germanium materials with the average mean free path $\lambda = 126$ nm [see Fig. 3(b)]. These results are consistent with our analysis in Sec. III C, namely, that the heat dissipation efficiency reaches the highest value when the spatial period P is approximately the phonon mean free path λ, i.e., $P^* \approx \text{Kn}$.

IV. THREE-DIMENSIONAL NANOCUBOID HEAT SOURCE

The 3D close-packed nanocuboid heat source is simulated in this section. As shown in Fig. 4(a), a number of nanocuboid heat sources are arranged periodically on the top of the substrate. The bottom of the 3D geometry is the heat sink with fixed temperature T_0 and the isothermal boundary condition is used [Eq. (B2)]. Its front and left views are both the same as the front view plotted in Fig. 1(a). The boundaries of the heat source and the top surface of the substrate are diffusely reflecting adiabatic boundaries [Eq. (B3)]. From the top view, there are two concentric squares with side lengths P and L_h and the boundaries of the substrate are all periodic. The lengths of the substrate and nanocuboid in the z direction are H and $h = H/8$, respectively. The basic settings are similar to those in quasi-2D hotspot systems [Fig. 1(a)]. At the initial moment $t = 0$, the temperature of the heat source is T_h and the temperature of the other surfaces is T_0. When $t > 0$, the heat dissipates from the heat source to the heat sink.

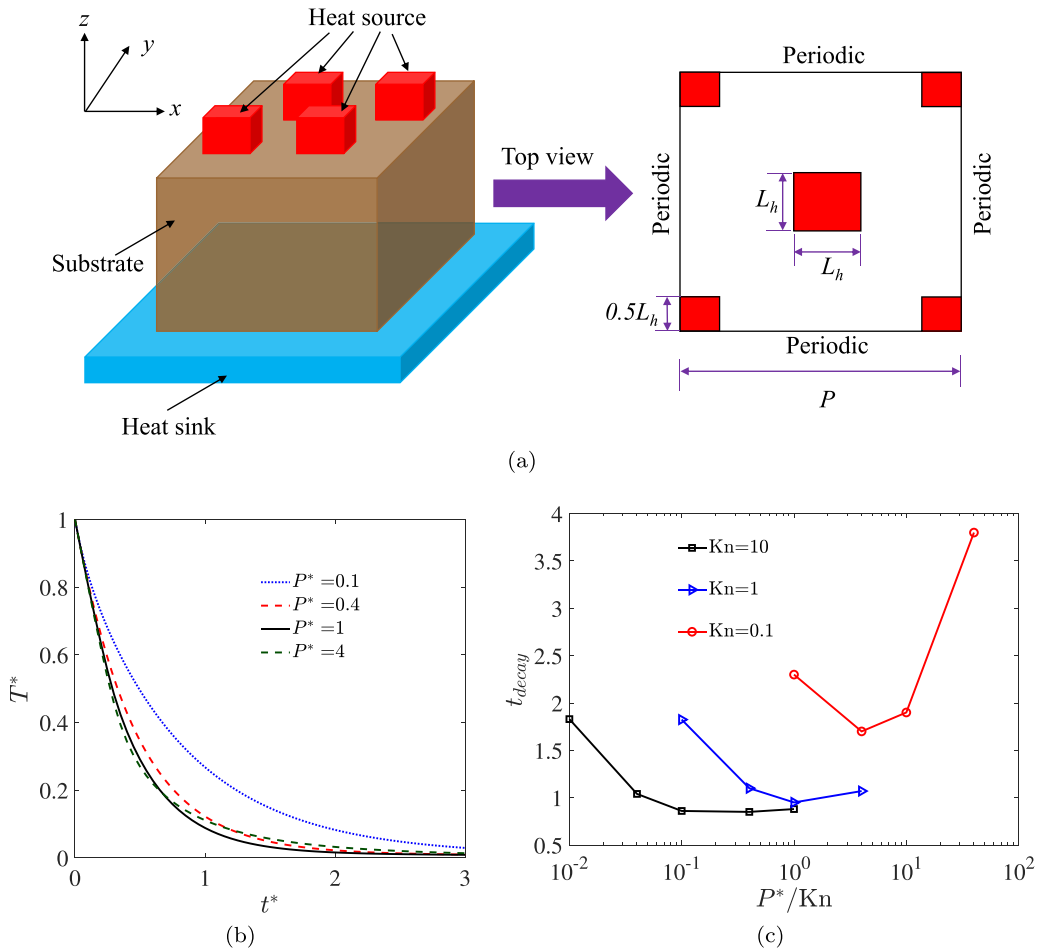

FIG. 5. (a) Schematic of the transient heat dissipation in a 3D nanocuboid heat source with a periodic staggered arrangement. (b) Heat dissipation process of the average temperature (7) based on the gray model, where Kn = 1. (c) Time decay t_{decay} with various P^* and Kn.

The detailed numerical solutions are shown in Appendix B. Due to the large computational amount, fewer numerical cases are simulated compared to those in quasi-2D hotspot systems and the frequency-independent BTE is solved. The thermal effects of phonon scattering and spatial period P are investigated. From Fig. 4 it can be found that the heat dissipation phenomena are similar to those in Fig. 1, namely, there is nonmonotonic heat dissipation phenomenon when the distance between two adjacent nanoscale hotspot decreases gradually. The fastest heat dissipation speed appears when $P^* \approx \mathrm{Kn}$.

In addition, changing the spatial distributions of nanocuboid heat sources, from a periodic array to a staggered arrangement, as shown in Fig. 5, numerical results show that this nonmonotonic heat dissipation phenomenon still exists. Thus, it can be concluded that the nonmonotonic heat dissipation phenomena are general in both close-packed quasi-2D and 3D hotspot systems.

V. CONCLUSION

In summary, the heat dissipation in close-packed quasi-2D nanoline and 3D nanocuboid hotspot systems has been studied based on the phonon BTE. Contrary to the previous intuitive understanding of micro- and nanoscale heat conduction, the present results have revealed that the heat dissipation efficiency is not monotonic with the distance between heat sources. The highest heat dissipation efficiency is reached when $P^*/\mathrm{Kn} \approx 1$. It is a result of the competition between the two processes: quasiballistic phonon transport when phonons escape from the nanoscale heat source and the scattering among phonons originating from the adjacent nanoscale heat source.

ACKNOWLEDGMENTS

This work was supported by the National Natural Science Foundation of China (Grant No. 12147122) and the China Postdoctoral Science Foundation (Grant No. 2021M701565). The authors acknowledge Chengyun Hua for useful communications on quasiballistic phonon transport. Computational resources were supported by the Center for Computational Science and Engineering of Southern University of Science and Technology.

APPENDIX A: NONLINEAR PHONON DISPERSION AND SCATTERING

The thermal contribution of optical phonons is small in room temperature silicon or germanium, so we only consider the longitudinal and transverse acoustic phonons (LA and

TABLE I. Quadratic phonon dispersion coefficients for silicon and germanium [43,44,51].

Material	Phonon	c_1 (10^5 cm/s)	c_2 (10^{-3} cm^2/s)
Si	LA	9.01	−2.0
Si	TA	5.23	−2.26
Ge	LA	5.63	−1.5
Ge	TA	2.60	−1.13

TA). The formulas in [51] are used to express the isotropic dispersion relations of the acoustic phonon branches,

$$\omega = c_1 k + c_2 k^2, \tag{A1}$$

where the wave vector $k \in [0, k_{\max}]$, $k_{\max} = 2\pi/A$ is the maximum wave vector in the first Brillouin zone, and A is the lattice constant. For silicon, $A = 0.543$ nm, and for germanium, $A = 0.565$ nm. The value of the group velocity is $v_g = c_1 + 2c_2 k$. The specific values of these coefficients in Eq. (A1) are shown in Table I.

Matthiessen's rule is used to calculate the effective relaxation time $\tau^{-1} = \tau_{\text{impurity}}^{-1} + \tau_U^{-1} + \tau_N^{-1} = \tau_{\text{impurity}}^{-1} + \tau_{NU}^{-1}$, where $\tau_{\text{impurity}}^{-1} = A_i \omega^4$. For the LA branch, $\tau_{NU}^{-1} = B_L \omega^2 T^3$; for the TA branch, when $0 \leqslant k < k_{\max}/2$, $\tau_{NU}^{-1} = B_T \omega T^4$, and when $k_{\max}/2 \leqslant k \leqslant k_{\max}$, $\tau_{NU}^{-1} = B_U \omega^2 / \sinh(\hbar\omega/k_B T)$. The specific values of these coefficients of relaxation time are shown in Table II. These input parameters of the phonon BTE have been validated by experiments [50] in previous studies [43,44].

APPENDIX B: NUMERICAL METHOD FOR THE BTE

The discrete unified gas kinetic scheme [52] is used to solve the phonon BTE numerically. Detailed introductions and numerical validations of this scheme were given in Refs. [10,17,18]. For quasi-2D nanoline hotspot systems, the spatial space is discretized with 90 uniform cells in the z direction and 40–200 uniform cells in the x direction. In silicon or germanium materials, the spatial space is discretized with $N_z = 90$ uniform cells in the z direction and $N_x = 40$–120 uniform cells in the x direction. Similarly, for the 3D nanocuboid hotspot systems, the spatial space is discretized with $N_z = 90$ uniform cells in the z direction and $N_x = N_y = 80$–200 uniform cells in both the x and y directions. The number of discretized cells in the x or y direction depends on the spatial period P. The larger the spatial period P is, the more discretized cells are used.

The phonon dispersion and scattering in silicon and germanium materials are given in Appendix A. For each of the phonon (LA and TA) branches, the wave vector is discretized into N_B equally and the midpoint rule is used for the numerical integration of the frequency space. In total, $2N_B$ discretized frequency bands are considered. Here we set $N_B = 20$.

The three-dimensional solid angle is $\boldsymbol{s} = (\cos\theta, \sin\theta\cos\varphi, \sin\theta\sin\varphi)$, where $\theta \in [0, \pi]$ is the polar angle and $\varphi \in [0, 2\pi]$ is the azimuthal angle. The $\cos\theta \in [-1, 1]$ is discretized with the N_θ-point Gauss-Legendre quadrature, while the azimuthal angular space $\varphi \in [0, \pi]$ (due to symmetry) is discretized with the $\frac{N_\varphi}{2}$-point Gauss-Legendre quadrature. In this study, we set $N_\theta \times N_\varphi = 40 \times 40$.

The van Leer limiter is used to deal with the spatial gradient of the distribution function and the time step is

$$\Delta t = \text{CFL} \times \frac{\Delta x}{v_{\max}}, \tag{B1}$$

where Δx is the minimum discretized cell size, CFL is the Courant-Friedrichs-Lewy number, and $v_{\max}$ is the maximum group velocity. In this simulation, CFL = 0.4.

The isothermal boundary condition is used for the heat sink, where the incident phonons are all absorbed and the phonons emitted from the boundary are in the equilibrium state with the boundary temperature T_{BC}. Its mathematical formula is

$$e(T_{\text{BC}}, \boldsymbol{s}, \omega) = C(T_{\text{BC}} - T_0), \quad \boldsymbol{s}\cdot\mathbf{n} > 0, \tag{B2}$$

where $\mathbf{n}$ is the normal unit vector of the boundary pointing to the computational domain. The diffusely reflecting adiabatic boundary condition controls the total heat flux across the boundary to be zero and phonons with the same frequency reflected from the boundary are equal along each direction. Its mathematical formula is

$$e(\boldsymbol{s}, \omega) = C(T_w - T_0), \quad \boldsymbol{s}\cdot\mathbf{n} > 0, \tag{B3}$$

where

$$T_w = T_0 + \frac{-\sum_p \iint_{\boldsymbol{s}'\cdot\mathbf{n}<0} v_g e \boldsymbol{s}'\cdot\mathbf{n}\, d\Omega\, d\omega}{\sum_p \iint_{\boldsymbol{s}\cdot\mathbf{n}>0} v_g C \boldsymbol{s}\cdot\mathbf{n}\, d\Omega\, d\omega}. \tag{B4}$$

TABLE II. Relaxation time coefficients for silicon and germanium [43,44].

Coefficient	Silicon	Germanium
A_i (s^3)	1.498×10^{-45}	2.40×10^{-44}
B_L (K^{-3})	1.180×10^{-24}	2.30×10^{-24}
B_T (K^{-3})	8.708×10^{-13}	3.0×10^{-12}
B_U (s)	2.890×10^{-18}	1.50×10^{-18}

APPENDIX C: INDEPENDENCE TESTS OF DISCRETE PARAMETERS

Independence tests of the discrete parameters in the whole phase space are conducted. First, the bulk thermal conductivity $\kappa_{\text{bulk}} = \sum_p \int C v_g^2 \tau/3 d\omega$ is used to find the optimized number of frequency bands. With different discretized numbers of the phonon frequency bands $N_B = 20, 40, 100$, the calculated bulk thermal conductivities of silicon at room temperature are all 145.9 W/m K. Similarly, the bulk thermal conductivity of germanium at room temperature is 58.8 W/m K. Hence the numerical integration in the phonon frequency space is regarded as converged when $N_B \geqslant 20$.

Second, the independence tests of the discretized solid angle space and time step are implemented, which is necessary to ensure that the ray effect and false scattering have little effect on the numerical results. We take the quasi-2D hotspot system [Fig. 1(a)] as an example. The ray effects usually appear in the ballistic regime, so we simulate the case with Kn = 10 and $P^* = 1$. The temporal evolution processes of

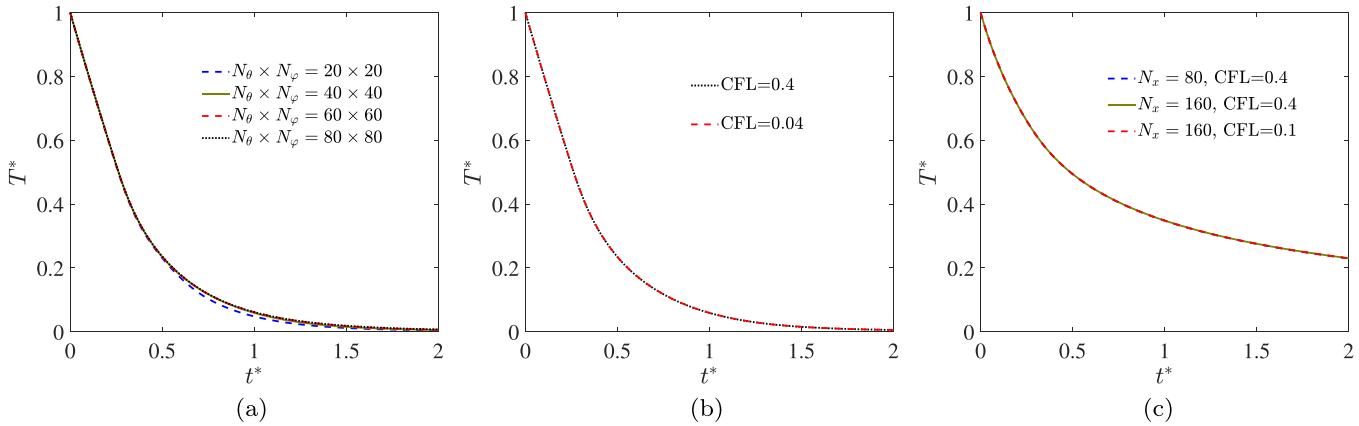

FIG. 6. Independence tests of the discrete parameters for the heat dissipation process of the average temperature (7) in the quasi-2D hotspot system, when $P^* = 1$. (a) Different numbers of discretized solid angles $N_\theta \times N_\varphi$, fixed discretized cells in the x direction $N_x = 80$, and fixed CFL number 0.4 for Kn = 10. (b) Different CFL number, fixed $N_\theta \times N_\varphi = 40 \times 40$, and fixed $N_x = 80$ for Kn = 10. (c) Different CFL numbers, different N_x, and fixed $N_\theta \times N_\varphi = 40 \times 40$ for Kn = 0.1.

the average temperature with different discretized solid angles and CFL numbers are plotted in Fig. 6. The numerical results confirm that the choice of $N_\theta \times N_\varphi = 40 \times 40$ and CFL = 0.4 are enough to accurately predict the transient ballistic heat conduction.

Finally, the discretized spatial cells are also tested. Usually, more discretized cells are needed near or in the diffusive regime, so we simulate the case with Kn = 0.1 and $P^* = 4$. Different discretized numbers in the x direction are tested and we find that 80 discretized cells in the x direction and CFL = 0.4 are adequate.

In summary, the present discretizations in Appendix B are accurate to capture the multiscale transient heat conduction in 3D materials.

[1] D. G. Cahill, W. K. Ford, K. E. Goodson, G. D. Mahan, A. Majumdar, H. J. Maris, R. Merlin, and S. R. Phillpot, J. Appl. Phys. **93**, 793 (2003).
[2] D. G. Cahill, P. V. Braun, G. Chen, D. R. Clarke, S. Fan, K. E. Goodson, P. Keblinski, W. P. King, G. D. Mahan, A. Majumdar *et al.*, Appl. Phys. Rev. **1**, 011305 (2014).
[3] A. L. Moore and L. Shi, Mater. Today **17**, 163 (2014).
[4] X. Gu, Y. Wei, X. Yin, B. Li, and R. Yang, Rev. Mod. Phys. **90**, 041002 (2018).
[5] R. J. Warzoha, A. A. Wilson, B. F. Donovan, N. Donmezer, A. Giri, P. E. Hopkins, S. Choi, D. Pahinkar, J. Shi, S. Graham, Z. Tian, and L. Ruppalt, J. Electron. Packag. **143**, 020804 (2021).
[6] Q. L. Yue, C. X. He, M. C. Wu, and T. S. Zhao, Int. J. Heat Mass Transf. **181**, 121853 (2021).
[7] Z. Zhang, Y. Ouyang, Y. Cheng, J. Chen, N. Li, and G. Zhang, Phys. Rep. **860**, 1 (2020).
[8] G. Chen, Nat. Rev. Phys. **3**, 555 (2021).
[9] A. Majumdar, J. Heat Transf. **115**, 7 (1993).
[10] C. Zhang and Z. Guo, Int. J. Heat Mass Transf. **134**, 1127 (2019).
[11] S. Xu, A. Fan, H. Wang, X. Zhang, and X. Wang, Int. J. Heat Mass Transf. **154**, 119751 (2020).
[12] Y. Ju and K. Goodson, Appl. Phys. Lett. **74**, 3005 (1999).
[13] T.-K. Hsiao, H.-K. Chang, S.-C. Liou, M.-W. Chu, S.-C. Lee, and C.-W. Chang, Nat. Nanotechnol. **8**, 534 (2013).
[14] C. W. Chang, D. Okawa, H. Garcia, A. Majumdar, and A. Zettl, Phys. Rev. Lett. **101**, 075903 (2008).
[15] X. Xu, L. F. C. Pereira, Y. Wang, J. Wu, K. Zhang, X. Zhao, S. Bae, C. T. Bui, R. Xie, J. T. L. Thong, B. H. Hong, K. P. Loh, D. Donadio, B. Li, and B. Özyilmaz, Nat. Commun. **5**, 3689 (2014).
[16] A. Beardo, M. López-Suárez, L. A. Pérez, L. Sendra, M. I. Alonso, C. Melis, J. Bafaluy, J. Camacho, L. Colombo, R. Rurali, F. X. Alvarez, and J. S. Reparaz, Sci. Adv. **7**, eabg4677 (2021).
[17] Z. Guo and K. Xu, Int. J. Heat Mass Transf. **102**, 944 (2016).
[18] X.-P. Luo and H.-L. Yi, Int. J. Heat Mass Transf. **114**, 970 (2017).
[19] G. D. Mahan and F. Claro, Phys. Rev. B **38**, 1963 (1988).
[20] G. Chen, J. Heat Transf. **118**, 539 (1996).
[21] P. G. Sverdrup, S. Sinha, M. Asheghi, S. Uma, and K. E. Goodson, Appl. Phys. Lett. **78**, 3331 (2001).
[22] M. E. Siemens, Q. Li, R. Yang, K. A. Nelson, E. H. Anderson, M. M. Murnane, and H. C. Kapteyn, Nat. Mater. **9**, 26 (2010).
[23] A. J. Minnich, J. A. Johnson, A. J. Schmidt, K. Esfarjani, M. S. Dresselhaus, K. A. Nelson, and G. Chen, Phys. Rev. Lett. **107**, 095901 (2011).
[24] Y. Hu, L. Zeng, A. J. Minnich, M. S. Dresselhaus, and G. Chen, Nat. Nanotechnol. **10**, 701 (2015).
[25] C. Zhang, D. Ma, M. Shang, X. Wan, J.-T. Lü, Z. Guo, B. Li, and N. Yang, Mater. Today Phys. **22**, 100605 (2022).
[26] M. N. Luckyanova, J. Mendoza, H. Lu, B. Song, S. Huang, J. Zhou, M. Li, Y. Dong, H. Zhou, J. Garlow, L. Wu, B. J. Kirby, A. J. Grutter, A. A. Puretzky, Y. Zhu, M. S. Dresselhaus, A. Gossard, and G. Chen, Sci. Adv. **4**, eaat9460 (2018).
[27] R. Hu, S. Iwamoto, L. Feng, S. Ju, S. Hu, M. Ohnishi, N. Nagai, K. Hirakawa, and J. Shiomi, Phys. Rev. X **10**, 021050 (2020).

[28] D. Ma, A. Arora, S. Deng, G. Xie, J. Shiomi, and N. Yang, Mater. Today Phys. **8**, 56 (2019).
[29] S. Lee, D. Broido, K. Esfarjani, and G. Chen, Nat. Commun. **6**, 6290 (2015).
[30] A. Cepellotti, G. Fugallo, L. Paulatto, M. Lazzeri, F. Mauri, and N. Marzari, Nat. Commun. **6**, 6400 (2015).
[31] S. Huberman, R. A. Duncan, K. Chen, B. Song, V. Chiloyan, Z. Ding, A. A. Maznev, G. Chen, and K. A. Nelson, Science **364**, 375 (2019).
[32] C. C. Ackerman, B. Bertman, H. A. Fairbank, and R. A. Guyer, Phys. Rev. Lett. **16**, 789 (1966).
[33] T. F. McNelly, S. J. Rogers, D. J. Channin, R. J. Rollefson, W. M. Goubau, G. E. Schmidt, J. A. Krumhansl, and R. O. Pohl, Phys. Rev. Lett. **24**, 100 (1970).
[34] K. M. Hoogeboom-Pot, J. N. Hernandez-Charpak, X. Gu, T. D. Frazer, E. H. Anderson, W. Chao, R. W. Falcone, R. Yang, M. M. Murnane, H. C. Kapteyn, and D. Nardi, Proc. Natl. Acad. Sci. USA **112**, 4846 (2015).
[35] T. D. Frazer, J. L. Knobloch, K. M. Hoogeboom-Pot, D. Nardi, W. Chao, R. W. Falcone, M. M. Murnane, H. C. Kapteyn, and J. N. Hernandez-Charpak, Phys. Rev. Applied **11**, 024042 (2019).
[36] L. Zeng and G. Chen, J. Appl. Phys. **116**, 064307 (2014).
[37] A. Beardo, J. L. Knobloch, L. Sendra, J. Bafaluy, T. D. Frazer, W. Chao, J. N. Hernandez-Charpak, H. C. Kapteyn, B. Abad, M. M. Murnane, F. X. Alvarez, and J. Camacho, ACS Nano **15**, 13019 (2021).
[38] H. Honarvar, J. L. Knobloch, T. D. Frazer, B. Abad, B. McBennett, M. I. Hussein, H. C. Kapteyn, M. M. Murnane, and J. N. Hernandez-Charpak, Proc. Natl. Acad. Sci. USA **118**, e2109056118 (2021).
[39] X. Chen, C. Hua, H. Zhang, N. K. Ravichandran, and A. J. Minnich, Phys. Rev. Applied **10**, 054068 (2018).
[40] C. Hua and A. J. Minnich, Phys. Rev. B **97**, 014307 (2018).
[41] J. Y. Murthy, S. V. J. Narumanchi, J. A. Pascual-Gutierrez, T. Wang, C. Ni, and S. R. Mathur, Int. J. Multiscale Comput. Eng. **3**, 5 (2005).
[42] H. Bao, J. Chen, X. Gu, and B. Cao, ES Energy Environ. **1**, 16 (2018).
[43] D. Terris, K. Joulain, D. Lemonnier, and D. Lacroix, J. Appl. Phys. **105**, 073516 (2009).
[44] V. Jean, S. Fumeron, K. Termentzidis, S. Tutashkonko, and D. Lacroix, J. Appl. Phys. **115**, 024304 (2014).
[45] C. Hua, L. Lindsay, X. Chen, and A. J. Minnich, Phys. Rev. B **100**, 085203 (2019).
[46] C. Zhang, Z. Guo, and S. Chen, Int. J. Heat Mass Transf. **130**, 1366 (2019).
[47] E. T. Swartz and R. O. Pohl, Rev. Mod. Phys. **61**, 605 (1989).
[48] J. Chen, X. Xu, J. Zhou, and B. Li, Rev. Mod. Phys. **94**, 025002 (2022).
[49] G. I. Barenblatt, *Dimensional Analysis* (CRC, Boca Raton, 1987).
[50] C. J. Glassbrenner and G. A. Slack, Phys. Rev. **134**, A1058 (1964).
[51] E. Pop, R. W. Dutton, and K. E. Goodson, J. Appl. Phys. **96**, 4998 (2004).
[52] Z. Guo and K. Xu, Adv. Aerodyn. **3**, 6 (2021).